ADVANCES IN COMPUTATIONAL TRANSONICS

VOLUME 4 IN THE SERIES
Recent Advances in Numerical Methods in Fluids

Edited by:

W. G. Habashi
Concordia University, Montreal, Canada
Consultant, Pratt & Whitney Canada

PINERIDGE PRESS
Swansea, U.K.

EULER SOLVERS AS AN ANALYSIS TOOL FOR AIRCRAFT AERODYNAMICS

Wolfgang Schmidt* and Antony Jameson+

*Dornier GmbH + Princeton University

1. INTRODUCTION

Aircraft development costs have escalated sharply during the last 20 years. Greater emphasis must be placed on exploring new configuration concepts aimed at expanding airplane performance capabilities by analytical and experimental techniques. The present state of the art in aerodynamic analysis and design requires extensive configuration iterations. Repeated wind tunnel testing is costly, time consuming, and relies heavily on inhouse experiences and expertise. Significant advances have been achieved in the last ten years in aerodynamic computational methods which allow the numerical simulation of flows around two- and three-dimensional configurations and components. They provide valuable guides to those seeking understanding of specific problems or those pursuing innovative design concepts.

It is the purpose of this chapter to discuss some numerical techniques for solving hyperbolic systems of partial differential equations which govern flows which can be solved by time or space marching. Solution methods for transonic potential flow which have been proved to be very useful, but are limited in application, have been reviewed in previous chapters. Here, the discussion is limited to solutions of the Euler equations, although the algorithms which are presented have been successfully applied also to the Navier Stokes equations [1].

To solve problems numerically, one must make several decisions. These include the following: (1) the selection of an appropriate form of the equations which describe the flow under consideration (2) an algorithm to calculate the numerical solution of the equations at interior points of the domain (3) a technique to properly approximate boundary conditions along the boundaries of the domain; and (4) the treatment of

shockwave or contact discontinuities which may occur within the domain. It is shown that a new combination of a finite volume discretization in conjunction with carefully designed dissipative terms, and Runge Kutta time stepping schemes, yields an effective method for solving the Euler equations in arbitrary geometric domains. Different types of acceleration techniques are proposed to improve the convergence speed of explicit time dependent methods. A large set of computational results shows the broad application of these methods.

2. GOVERNING SET OF DIFFERENTIAL EQUATIONS

Within the scope of this study we consider only flows governed by first-order hyperbolic systems of partial differential equations. Such a system can be written in general form in an N-dimensional space $X = (x_1, x_2, \ldots, x_{N-1}, t)$ as

$$\frac{\partial U}{\partial t} + \sum_{j=1}^{N-1} \left(C_j \frac{\partial F_j}{\partial x_j} + E_j \right) = 0 \qquad (1)$$

where U and E_j are vectors of dimension M; F_j is a vector of dimension M_j, and C_j is an $M \times M_j$ matrix. The coordinate t is the coordinate direction in which the solution is advanced. t can be either a time or space coordinate. U is the solution or state vector of the system. Given the initial conditions at $t = t_o$, we seek to solve for $U(x_1, x_2, \ldots, x_{N-1}, t)$ for $t > t_o$. In general, C_j, F_j, E_j are functions of the space X and the elements of U. Letting I represent the identity matrix and ϕ the null vector (vector whose elements are all zero) we say that Eq. (1) is written in strong conservation form (or divergence law form) if $C_j = I$ and $E_j = \phi$ for all j, or weak conservation form if $C_j = I$ for all j. Otherwise, Eq. (1) is said to be in nonconservation form. In the following sections only solution methods for the equations in conservation form will be discussed.

2.1 Time-Dependent Euler Equations

The time-dependent Navier Stokes equations reduce to the Euler equations for inviscid flow if the stress tensor $\bar{T}$ only contains a normal stress as the pressure p and if the heat conductivity is zero. The system of time-dependent equations written in strong conservation form for mass, momentum, and energy in a Cartesian coordinate system of three spatial dimensions (x,y,z) is

$$\frac{\partial U}{\partial t} + \frac{\partial F_1}{\partial x} + \frac{\partial F_2}{\partial y} + \frac{\partial F_3}{\partial z} = 0 \qquad (2)$$

where N has been taken as 4 and

$$U = \begin{Bmatrix} \rho \\ \rho u \\ \rho v \\ \rho w \\ E \end{Bmatrix}, \quad F_1 = \begin{Bmatrix} \rho u \\ \rho u^2 + p \\ \rho v \\ \rho w \\ (E+p)\, u \end{Bmatrix}, \quad F_2 = \begin{Bmatrix} \rho v \\ \rho uv \\ \rho v^2 + p \\ \rho vw \\ (E+p)\, v \end{Bmatrix}, \quad F_3 = \begin{Bmatrix} \rho w \\ \rho uw \\ \rho vw \\ \rho w^2 + p \\ (E+p)\, w \end{Bmatrix} \tag{3}$$

The marching coordinate is the time t. The velocities in the coordinate directions x, y, z are represented by u, v, w and the pressure p is obtained from an equation of state as a function of density ρ and specific internal energy e

$$e = \frac{E}{\rho} - \frac{u^2 + v^2 + w^2}{2} \tag{4}$$

where E is the total energy. For an ideal gas, where the ratio of the specific heats γ is a constant, the equation of state is

$$p = (\gamma - 1)\, \rho e \tag{5}$$

Other examples for real gases are shown in Ref. 2.

2.2 Transformed Equations

It is often convenient for both analytical and/or computational purposes to transform a system of equations into a new coordinate system more natural to the fluid domain. One simple example is the transformation into a cylindrical coordinate system (see, e.g. Kutler at al in Ref. 3). For more general curvilinear coordinate systems these transformations become very complex. However, as shown by Viviand in Ref. 4, this will not change the conservation properties of the governing equations. Since we will only discuss finite volume methods in the present paper, no coordinate transformation is needed, as is shown in the following section.

2.3 Finite Volume Approach

The form we now consider is the integral form of a system of hyperbolic equations which can be expressed in conservation form. It is a useful form for both physical and computational purposes. If the hyperbolic system is expressed as

$$\frac{\partial \vec{U}}{\partial t} + \sum_{j=1}^{N-1} \frac{\partial \vec{F}_j}{\partial x_j} = 0 \tag{6}$$

then by defining the flux-tensor $\bar{\bar{H}} = \sum_{j=1}^{N-1} \vec{F}_j \vec{i}_j$, where $\vec{i}_j$ are unit vectors in the x_j coordinate directions, we can rewrite the system as

$$\frac{\partial \vec{U}}{\partial t} + \nabla \bar{\bar{H}} = 0 \tag{7}$$

Integrating this equation within a volume V enclosed by the surface S yields

$$\frac{\partial}{\partial t} \int_V \vec{U} dv + \int_S \bar{\bar{H}} ds = 0 \tag{8}$$

for volumes or meshes fixed in time where the direction of $\vec{ds}$ is that of the outer normal to the surface S. For meshes moving in time Eq. (8) has to be written as

$$\frac{\partial}{\partial t} \int_{V(t)} \vec{U} dv + \int_{S(t)} \bar{\bar{H}} \vec{ds} - \int_{S(t)} \vec{U} \cdot \vec{\lambda}\, \vec{ds} = 0 \tag{9}$$

with $\vec{\lambda}$ as local velocity of ds (mesh velocity).

Eq. (8) and (9) express the total flux balance in a control volume. They describe the natural physical model of conservation of mass, momentum and energy within a discrete volume.

2.4 Relation at Discontinuities

Following the analysis of Lax [5], a solution of a system of differential equations in a domain is called genuine if it and its first partial derivatives are continuous everywhere in the domain D. A weak solution is also a solution of the system but is genuine only in subdomains of D. The subdomains are separated by surfaces in D across which the solution is allowed to be discontinuous. Relations governing jumps in the values of the dependent variables across discontinuities may be obtained for systems in conservation form by integrating the system about a small volume containing a portion of the surface. For example, a surface of slope tan ϕ in the (x_j, x_α) plane is shown in Fig. 1.

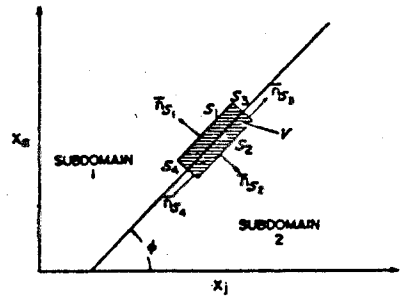

Fig. 1: Two subdomains separated by a surface at which the solution F_α is discontinuous.

For simplicity, the surface is assumed to be orthogonal to all the other coordinate directions. Using the conservation equations from the previous chapter we obtain with the areas of the surfaces S_3 and $S_4 \to 0$:

$$F_{\alpha_1} \vec{i}_\alpha \cdot \vec{n}_{S_1} + F_{j_1} \vec{i}_j \cdot \vec{n}_{S_1} + F_{\alpha_2} \cdot \vec{i}_\alpha \cdot \vec{n}_{S_2} + F_{j_2} \cdot \vec{i}_j \cdot \vec{n}_{S_2} = 0$$

or

$$(F_{\alpha_2} - F_{\alpha_1}) \ (\tan\phi)^{-1} = F_{j_2} - F_{j_1}$$

The above jump relation is commonly known as the Rankine-Hugoniot equation. If $x_\alpha = t$, then $(\tan\phi)^{-1} = U_S$, the speed of the discontinuity (shock wave speed), and the relation determines the jump across a moving discontinuity. If x_α is a spatial coordinate, the relation specifies the jump across a steady oblique discontinuity.

3. NUMERICAL DISCRETISATION

The discretization procedure which we propose for Eq. (8) or (9) follows the method of lines in decoupling the approximation of the spatial and time dependent terms. The computational domain is divided into quadrilateral cells for two-dimensional flows or hexahedrons for three-dimensional flows. For simplicity the spatial discretization will be dicussed for two-dimensional flows only.

A system or ordinary differential equations is obtained by applying Eq. (8) or (9) to each cell separately. The resulting equations can then be solved by several alternative time stepping schemes. The present paper will only discuss central approximations and Runge-Kutta-type stepping schemes since they proved to be extremely effective in practice. The most

widely used schemes are those of MacCormack, e.g. see Ref. [6[, or Lax-Wendroff [7]. Detailed descriptions of these schemes can be found in the cited literature.

3.1 Central Space Approximations

The physical space is discretised into a mesh of quadrilateral cells as sketched in Fig. 2

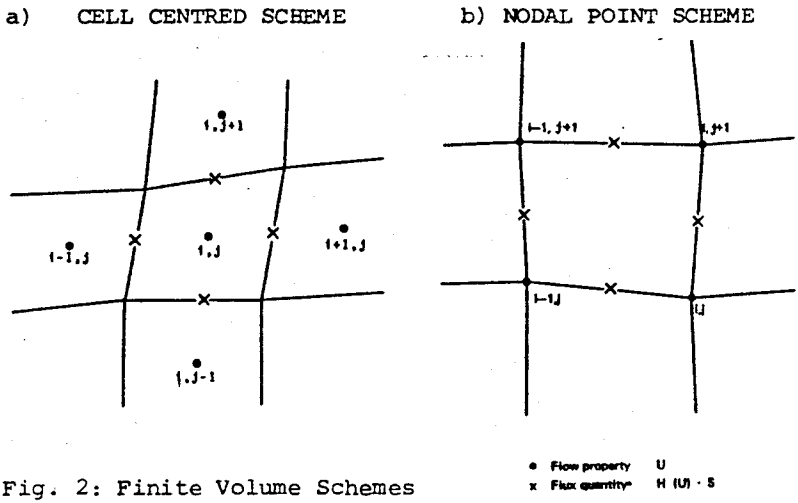

Fig. 2: Finite Volume Schemes

Let the values of the quantities associated with each cell be denoted by i, j. Fig. 2a represents a cell-centered scheme where these can be regarded as values at the cell center, or

$$U_{i,j} = \frac{\iint U\,dvol}{\iint dvol} \tag{10}$$

For each cell Eq. (8) can be expressed as

$$\frac{d}{dt}(UV) + Q \cdot U = 0 \tag{11}$$

where V is the cell area, and the operator Q represents an approximation to the boundary integral defined by the second integral in Eq. (8). This is defined as follows. Let Δx_k and Δy_k be the movements of x and y along side k of the cell, with appropriate signs. Then the flux balance for, say, the x-momentum component, is represented as

$$\frac{\partial}{\partial t}(\rho u) + \sum_{k=1}^{4} (Q_k \rho u_k + \Delta y_k \cdot p_k) = 0 \tag{12}$$

Where Q_k is the flux velocity

$$Q_k = \Delta y_k u_k - \Delta x_k v_k \tag{13}$$

and the sum is over the four sides of the cell. Each quantity such as ρ_2 or $(\rho u)_2$ is evaluated as the average of the values in the cells on the two sides of the face. For example

$$(\rho u)_2 = \frac{1}{2}\{(\rho u)_{i,j} + (\rho u)_{i+1,j}\} \tag{14}$$

The scheme reduces to a central difference scheme on a Cartesian grid, and is second order accurate provided that the mesh function is smooth enough.

A similar nodal point scheme can be constructed as shown in Fig. 26. Now all U are defined in the nodal points i,j, itself and the first integral in Eq. (8) is approximated as

$$\frac{d}{dt}\int_V U d\text{vol} = \frac{d}{dt}\{\frac{1}{4}(U_{i,j}+U_{i-1,j}+U_{i,j-1}+U_{i-1,j-1}) \cdot V\} \tag{15}$$

Consequently, the quantities such as ρ_2, ρu_2 are now evaluated as the averages

$$(\rho u)_2 = \frac{1}{2}\{(\rho u)_{i,j-1} + (\rho u)_{i,j}\} \tag{16}$$

3.2 Dissipative Terms

To suppress the tendency for odd and even point decoupling, and to prevent the appearance of wiggles in region containing severe pressure gradients in the neighborhood of shock waves or stagnation points, it proves necessary to augment the finite volume scheme by the addition of artificial dissipative terms. Therefore equation (11) is replaced by the equation

$$\frac{d}{dt}(UV) + QU - DU = 0 \tag{17}$$

where Q is the spatial discretization operator defined by equations (12-14), and D is a dissipative operator. Extensive numerical experiments have established that an effective form for DW is a blend of second and fourth differences with coefficients which depend either on the local gradient of the static or total pressure or else on the local entropy production rate.

The construction of the dissipative terms for each of the four dependent variables is similar. For the density equation

$$D\rho = D_x\rho + D_y\rho \tag{18}$$

where $D_x\rho$ and $D_y\rho$ are corresponding contributions for the two coordinate directions, written in conservation form

$$D_x\rho = \{d_{i+1/2,j} - d_{i-1/2,j}\} \tag{19}$$

$$D_y\rho = \{d_{i,j+1/2} - d_{i,j-1/2}\}$$

The terms on the right all have a similar form: for example

$$d_{i+1/2,j} = \frac{V_{i+1/2,j}}{\Delta t} \left\{ \begin{array}{l} \varepsilon^{(2)}_{i+1/2,j} \ (\rho_{i+1,j} - \rho_{i,j}) \\ \\ -\varepsilon^{(4)}_{i+1/2,j} \ (\rho_{i+1,j} - 3\rho_{i+1,j} + 3\rho_{i,j} - \rho_{i-1,j}) \end{array} \right. \tag{20}$$

where V is the cell volume, and the coefficients $\varepsilon^{(2)}$ and $\varepsilon^{(4)}$ are adapted to the flow. Define

$$\nu_{i,j} = - \frac{|F_{i+1,j} - 2F_{i,j} + F_{i-1,j}|}{|F_{i+1,j}| + 2\,|F_{i,j}| + |F_{i-1,j}|} \tag{21}$$

where F can be either static pressure p, total pressure p_i, or a measure for entropy.

Then

$$\varepsilon^{(2)}_{i+1/2,j} = \kappa^{(2)} \max\ (\nu_{i+1,j}, \nu_{i,j}) \tag{22}$$

and

$$\varepsilon^{(4)}_{i+1/2,j} = \max\ \{0, \ (\kappa^{(4)} - \varepsilon^{(2)}_{i+1/2,j})\} \tag{23}$$

where typical values of the constants $\kappa^{(2)}$ and $\kappa^{(4)}$ are

$$\kappa^{(2)} = \frac{1}{4},\ \kappa^{(4)} = \frac{1}{256} \quad \text{for } F = p \quad \text{or } \kappa^{(2)} = 2.5 \text{ for } F$$

based on entropy.

The dissipative terms for the remaining equations are obtained by substituting ρu, ρv and E for ρ in these formulas.

The scaling $V/\Delta t$ in equation (19) conforms to the inclusion of the cell area V in the dependent variables of equation (11). Since equation (19) contains undivided differences, it follows that if $\varepsilon^{(2)} = O(\Delta x^2)$ and $\varepsilon^{(4)} = O(\Delta x^4)$, then the added terms are of order Δx^3. This will be the case in a region where the flow is smooth. Near a shock wave $\varepsilon^{(2)} = O(\Delta x)$, and the scheme behaves locally like a first order accurate scheme.

It has been found that in smooth regions of the flow, the scheme is not sufficiently dissipative unless the fourth differences are included, with the result that calculations will generally not converge to a completely steady state. Instead, after they have reached an almost steady state, oscillations of very low amplitude continue indefinitely (with $\max \left(\frac{\partial \rho}{\partial t}\right)_{\text{local}} \sim 10^3$, for example).

Near shock waves it has been found that the fourth differences tend to induce overshoots, and therefore they are switched off by subtracting $\varepsilon^{(2)}$ from $\kappa^{(4)}$ in equation (22).

Numerous numerical experiments have proven that this type of dissipation produce insignificantly small total pressure losses or entropy changes.

Special attention has to be given to the formulation of the dissipative terms near boundaries. Improper treatment will lead to distortions of the flux balances which will not conserve circulation, for example, and may result in the wrong lift.

3.3 Time Stepping Schemes

Stable time stepping methods for equation (10) can be patterned on standard schemes for ordinary differential equations. Multistage two level schemes of the Runge Kutta type have the advantage that they do not require any special starting procedure, in contrast to leap frog and Adams Bashforth methods, for example. The extra stages can be used either

(1) to improve accuracy, or
(2) to extend the stability region.

An advantage of this approach is that the properties of these schemes have been widely investigated, and are readily available in textbooks on ordinary differential equations.

Consider a linear system of equations

$$\frac{dU}{dt} + AU = 0 \tag{24}$$

Suppose that A can be expressed as $A = T\Lambda T^{-1}$ where T is the matrix of the eigenvectors of A, and Λ is diagonal. Then setting $v = V^{-1}U$ yields separate equations

$$\frac{d}{dt} v_k + \lambda_k v_k = 0 \tag{25}$$

for each dependent variable v_k. The stability region is that region of the complex plane containing values of $\lambda\Delta t$ for which the scheme is stable. Consider now the model problem

$$\frac{\partial u}{\partial t} + a \frac{\partial u}{\partial x} + \varepsilon\Delta x \frac{\partial^2 u}{\partial x^2} = 0 \tag{26}$$

on an uniform mesh with interval Δx, with a dissipative term of order Δx. This can be reduced to a system of ordinary differential equations by introducing central-difference approximations for $\frac{\partial}{\partial x}$ and $\frac{\partial^2}{\partial x^2}$:

$$\frac{du_i}{dt} + \frac{a}{\Delta x}(u_{i+1} - u_{i-1}) + \frac{\varepsilon}{\Delta x}(u_{i+1} - 2u_i - u_{i-1}) = 0 \tag{27}$$

Taking the Fourier transform in space

$$\hat{u} = \frac{1}{2\pi} \int_{-\infty}^{\infty} u e^{i\omega x}\, dx \tag{28}$$

this becomes

$$\frac{d\hat{u}}{dt} + \lambda\hat{u} = 0 \tag{29}$$

where

$$\lambda = \frac{1}{\Delta x}\left(i\, a \sin \omega\Delta x - 4\varepsilon \sin^2 \frac{\omega\Delta x}{2}\right) \tag{30}$$

It can be seen that the maximum allowable value of the imaginary part of $\lambda\Delta t$ determines the maximum value of the Courant number a $\{\frac{\Delta x}{\Delta t}\}$ for which the calculation will be stable, while the addition of the dissipative term shifts the region of interest to the left of the imaginary axis.

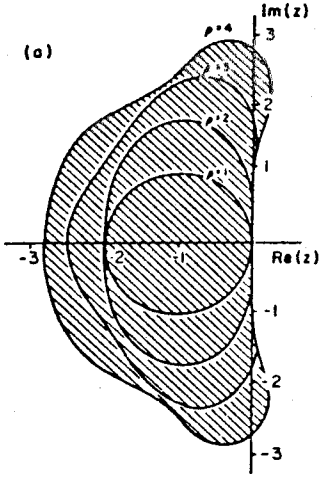

(a) standard schemes of order 1,2,3,4 (Stetter, 1973)

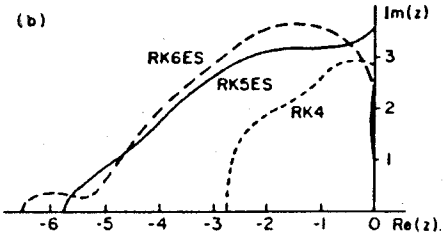

(b) non-standard schemes of order 4,5,6 (Lawson, 1966)

Fig. 3 Stability regions for various Runge-Kutta time-stepping schemes

In the present case, if the grid is held fixed in time so that the cell area V is constant, the system of equations (11) has the form

$$\frac{dU}{dt} + PU = 0 \tag{31}$$

where if Q is the discretization operator defined in Section 3.1, and D is the dissipative operator defined in Section 3.2, the nonlinear operator P is defined as

$$PU \equiv \frac{1}{V}(QU - DU) \tag{32}$$

Our investigations so far have concentrated on time stepping schemes with three to six stages. Since three stage schemes are discussed by A. Rizzi in a following chapter of the present book, we limit ourselves to the four stage scheme which we have found to be the most efficient one so far. Variations of the three stage scheme have been proposed by Gary [8], Stetter [9], and Graves and Johnson [10]. It can be regarded as a Crank Nicolson scheme with a fixed point iteration

to determine the solution at time level n+1, and the iterations terminated after the third iteration. It is second order accurate in time.

The scheme which has been extensively investigated is the classical fourth order Runge Kutta scheme, defined as follows: At time level n set

$$
\begin{aligned}
U^{(0)} &= U^n \\
U^{(1)} &= U^{(0)} - \frac{\Delta t}{2} PU^{(0)} \\
U^{(2)} &= U^{(0)} - \frac{\Delta t}{2} PU^{(1)} \\
U^{(3)} &= U^{(0)} - \Delta t\, PU^{(2)} \\
U^{(4)} &= U^{(0)} - \frac{\Delta t}{6} (PU^{(0)} + 2PU^{(1)} + 2PU^{(2)} + PU^{(3)}) \\
U^{n+1} &= U^{(4)}
\end{aligned}
\tag{33}
$$

Variations can be obtained by using different coefficients in the stages.

These schemes are fourth order accurate in time, and for the model problem (25) with $\varepsilon = 0$, they are stable for Courant numbers

$$\left|\frac{a\Delta t}{\Delta x}\right| \leq 2\sqrt{2}$$

Its stability region, which is displayed in Fig. 3 taken from page 176 of Ref. [9], for example, also extends well to the left of the imaginary axis, allowing latitude in the introduction of dissipative terms.

All these schemes have the property that if $PU^n = 0$ then $U^{(1)} = U^{(0)}$, and so on, so that $U^{n+1} = U^n$ and the steady state solution is

$$PU = 0$$

independent of the time step Δt. This allows a variable time step determined by the bound on the local Courant number to be used to accelerate convergence to a steady state without altering the steady state.

The expense of re-evaluating the dissipative terms at every stage of these schemes is substantial. One method of avoiding this is to introduce the dissipative terms in a separate fractional step after the last stage of the Runge Kutta

scheme. Then equation (32) is replaced by

$$PU \equiv \frac{1}{V} QU \tag{34}$$

and the fourth order Runge Kutta scheme defined by equation (33), for example, is modified by setting

$$U^{n+1} = U^{(4)} + \frac{\Delta t}{V} DU^{(4)} \tag{35}$$

This method has the advantage that the stability properties for the two fractional steps are independent, so that the scheme will be stable if each fractional step is stable. It has the disadvantage that the steady state solution is no longer independent of the time step.

An alternative approach which has proved successful in practice, is to freeze the dissipative terms at their values in the first stage. Thus the fourth order Runge Kutta scheme is modified so that it has the form

$$\begin{aligned}
U^{(0)} &= U^n \\
U^{(1)} &= U^{(0)} - \frac{\Delta t}{2V} QU^{(0)} + \frac{\Delta t}{2V} DU^{(0)} \\
U^{(2)} &= U^{(0)} - \frac{\Delta t}{2V} QU^{(1)} + \frac{\Delta t}{2V} DU^{(0)} \\
U^{(3)} &= U^{(0)} - \frac{\Delta t}{V} QU^{(2)} + \frac{\Delta t}{V} DU^{(0)} \\
U^{(4)} &= U^{(0)} - \frac{\Delta t}{6V} (QU^{(0)} + 2QU^{(1)} + 2QU^{(2)} + QU^{(3)}) + \frac{\Delta t}{V} DU^{(0)}
\end{aligned} \tag{36}$$

The operators Q and D require roughly equal amounts of computation. Assigning to each 1 unit of work, and assuming that dissipative terms would be required in the leap frog or Mac Cormack schemes, both of which have maximum time steps bounded by a Courant number of one, one obtains the following table for the relative efficiency of the schemes:

Scheme	Evaluations of QU	Evaluations of DU	Maximum Work	Maximum Courant Number	Efficiency = time step / work
Leap frog	1	1	2	1	1/2
MacCormack	2	1	3	1	1/3
3 stage	3	3	6	2	1/3
4 stage	4	4	8	2.8	.35
4 stage (frozen DU)	4	1	5	2.8	.56

3.4 Boundary Conditions

Improper treatment of the boundary conditions can lead to serious errors and perhaps instability. In order to treat the flow exterior to a profile one must introduce an artificial outer boundary to produce a bounded domain. If the flow is subsonic at infinity there will be three incoming characteristics where there is inflow across the boundary, and one outgoing characteristic, corresponding to the possibility of escaping acoustic waves. Where there is outflow, on the other hand, there will be three outgoing characteristics and one incoming characteristic. According to the theory of Kreiss [11], three conditions may therefore be specified at inflow, and one at outflow, while the remaining conditions are determined by the solution of the differential equation. It is not correct to specify free stream conditions at the outer boundary.

For the formulation of the boundary conditions it is convenient to assume a local transformation to coordinates X and Y such that the boundary coincides with a line Y = constant. Using subscripts X and Y to denote derivatives, the Jacobian

$$h = x_X y_Y - x_Y y_X \tag{37}$$

corresponds to the cell area of the finite volume scheme. Introduce the transformed flux vectors

$$G_1 = y_Y F_1 - x_Y F_2, \qquad G_2 = x_X F_2 - y_X F_1 \tag{38}$$

where F_1 and F_2 are defined by Eq. (2). In differential form Eq. (2) then becomes

$$\frac{\partial}{\partial t}(hU) + \frac{\partial G_1}{\partial X} + \frac{\partial G_2}{\partial Y} = 0 \tag{39}$$

a. Far Field Conditions

Stable boundary conditions have been given by Gottlieb and Turkel [12] and Gustafsson and Oliger [13] for a variety of difference scheme. The treatment of the outer boundary condition adopted here follows similar lines. The equations are linearized about values at the end of the previous time step, and the characteristic variables corresponding to outgoing characteristics are then determined by extrapolation from the interior, while the remaining boundary conditions are specified in a manner consistent with the conditions imposed by the free stream. Let

$$A = \frac{\partial G_1}{\partial U} , \quad B = \frac{\partial G_2}{\partial U} \tag{40}$$

Since the boundary is a line Y = constant, the eigenvalues of B determine the incoming and outgoing characteristics. If q_n and q_t are the velocity components normal and tangential to the boundary, and c is the speed of sound, these eigenvalues are q_n, q_t, q_n-c, and q_n+c. Let values at the end of the previous step be denoted by the subscript o, and let T_o be the eigenvector matrix of B_o. Then B_o is reduced to diagonal form by the transformation $\Lambda_o = T_o^{-1} B_o T_o$, and setting $v = T_o^{-1} U$ the linearized equation assumes the form

$$\frac{\partial}{\partial t}(hv) + T_o^{-1} A_o T_o \frac{\partial v}{\partial X} + \Lambda_o \frac{\partial v}{\partial y} = 0 \tag{41}$$

The characteristic variables are the components of v. These are $p-c_o^2\rho$, q_t, $p-\rho_o c_o q_n$ and $p_o+\rho_o c_o q_n$.

Let values extrapolated from the interior and free stream values be denoted by the subscripts e and ∞. Then at the inflow boundary we set

$$p - c_o^2\rho = p_\infty - c_o^2\rho_\infty \tag{42a}$$

$$q_t = q_{t_\infty} \tag{42b}$$

$$p - \rho_o c_o q_n = p_\infty - \rho_o c_o q_{n_\infty} \tag{42c}$$

$$p + \rho_o c_o q_n = p_e + \rho_o c_o q_{n_e} \tag{42d}$$

yielding

$$p = \frac{1}{2}\left(p_e + p_\infty + \rho_o c_o \left(q_{n_e} - q_{n_\infty}\right)\right) \tag{43}$$

$$q_n = q_{n_\infty} + \frac{p - p_\infty}{\rho_o c_o}$$

The density can be determined from (42a). For steady state calculations it can alternatively be determined by specifying that the total enthalpy H has its free stream value.

At the outflow boundary one condition should be specified. If the flow is a parallel stream then $\frac{\partial p}{\partial y} = 0$, so for an open domain

$$p = p_\infty \tag{44}$$

A non reflecting boundary condition which would eliminate incoming waves is

$$\frac{\partial}{\partial t}\left(p - \rho_o c_o q_n\right) = 0 \tag{45}$$

This does not assure (44). Following Rudy and Strikwerda [14], Eq. (44) and (45) are therefore combined as

$$\frac{\partial}{\partial t}\left(p - \rho_o c_o q_n\right) + \alpha(p - p_\infty) = 0 \tag{46}$$

where a typical value of the parameter α is 1/8. The velocity components and energy are extrapolated from the interior.

A very simple set of quite efficient boundary conditions can be found by using the flux variables plus the characteristics to decide upon the number of conditions to be specified. For flows entering the fluid domain at a boundary only one variable can be extrapolated from inside, e.g. density. If total enthalpy, flow direction, and total pressure are prescribed at the boundary, ρu, ρv, and p can be computed. For flows leaving the fluid domain a set of exit conditions is derived by prescribing only static pressure p, extrapolating ρu, ρv, E, and computing ρ from the energy equation.

For turbomachinery cascades only periodicity-conditions have to be applied rather than the external far field conditions.

For cases with detached bow shocks it can be desirable to use a moving mesh aligned with the bow shock for better ac-

curacy. All the relations discussed in the previous chapter apply also for such cases if Eq. (9) is discretized. Only the mesh velocity based on the moving bow shock is required as additional information. Basically, two solution processes are of practical use:

- characteristic relations; for details see Ref. [16] and [17] for two-dimensional flows and Ref. [18] for three space dimensions

- extrapolation of the pressure from inside the domain to the rearward facing side of the shock and application of the classical shock relations as discussed in section 2.4.

Comparisons of both approaches in Ref. 19 indicate that the second approach especially in three space dimensions is superior due to its much easier and faster coding for nearly the same accuracy.

Various other boundary conditions designed to reduce reflections from the outer boundary have been proposed by several authors [19], [20], but it seems that although it would be worth while to test some more alternatives, the proper treatment of the dissipative terms described in section 3.2 at the outer boundaries is much more important, especially for lifting flows. The violation of flux balance at the boundaries can cause serious circulation losses.

Since the full equations of motion do not have any built-in mechanism to conserve circulation as for instance full potential methods; the far field has to be placed either far enough away to permit the flow direction upstream to be undisturbed, or a vortex term has to be added at the boundary. For three-dimensional flows with longitudinal vortices the downstream pressure can not be set constant any more but must allow for variation in the cross flow plane based on the velocity distribution.

b. Body Boundary Conditions

Consider first the boundary condition at the solid wall.

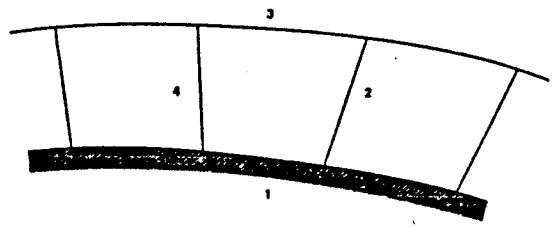

Fig. 4: Mesh Arrangement at Body Boundary

Across side 1 of cell A in the sketch there is no convected flux since

$$x_X v - y_X u = 0 \tag{47}$$

But there are contributions Δyp and Δxp to the momentum equations, which require an estimate of the pressure at the wall. Taking the time derivative of {equation (47) multiplied by ρ}, and substituting for $\frac{\partial}{\partial t}(h\rho u)$ and $\frac{\partial}{\partial t}(h\rho v)$ from equation (39) leads to the relation given by Rizzi in Ref. [21]

$$(x_X^2+y_X^2)\, p_y = (x_X x_Y+y_X y_Y)\, p_X + \rho\,(y_Y u - x_Y v)\,(v x_{XX} + u y_{XX}) \tag{48}$$

Thus we can estimate p_y in terms of quantities which can be determined from the interior solution, and we can use this value of p_y to extrapolate the pressure from the adjacent cell center to the wall. This approach is also called "normal momentum method". Further techniques are described in Ref. [22] by MacCormack. For fine meshes, the simple $p_b = p_1$ approach proved to be accurate enough for engineering purposes.

Numerical experiments over some time proved the wall pressure estimation to be the most critical one on standard meshes for spurious entropy production. Regions of large curvature along with high streamwise velocity gradients can experience fairly large total pressure losses which form thin "viscous layers". These effects are not caused by the numerical dissipation as described in section 3.2 but only by the p-extrapolation formula. In fact, the previously described normal momentum formula only gives good results if the first cells outside the body form a very thin row of volumes. Improved results which are less mesh dependent can be obtained by the first order extrapolation formula for the body pressure

$$p_b = 1.5\, p_1 - 0.5\, p_2 \tag{49}$$

A wide range of different formulas has been analysed numerically in Ref. [23]. The main conclusions are that all wall pressure formulas which require differentials of the metrics of the body need special care in mesh generation.

3.5 Kutta Conditions for Lifting Flows

In potential flow theory, Kutta conditions are needed at all surfaces where the flow is leaving the contour, e.g. at trailing edges, side edges. In two-dimensional lifting airfoil flow the classical Kutta-condition says that the static pressure at the trailing edge on upper and lower is equal and thus the velocity vector is equal in magnitude and direction since in isentropic flow total pressure is constant. This leads

to zero velocity at the trailing edge for nonzero trailing edge angle. For three-dimensional lifting flow Mangler and Smith in Ref. [24] discuss in detail possible solutions and trailing edge wakes behind wings. All standard methods in linear and nonlinear compressible potential flow theory assume the wake, and thus the lines with the jump in potential, to leave in the bisector-direction and to have constant jumps in potential along x in spanwise constant locations. The flow around the wing tip in general is neglected. This can cause at higher lift coefficients quite large deviations from the physically correct situation.

Solutions to the full compressible Euler equations do not need any explicit Kutta-condition to be unique, neither in two- nor in three-dimensional flow. Numerous examples have been presented by different authors, e.g. Ref. [25] and [26]. This might be explained on the basis of Fig. 5 and 6. Potential flow needs for uniqueness a Kutta condition, since all rear stagnation point locations are possible. As sketched in Fig. 5, for all points q = 0 and static pressure p = stagnation pressure p_t is a solution. So this point has to be specified by an additional condition.

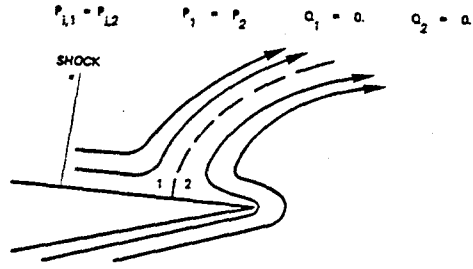

Fig. 5: Trailing edge flow in isentropic potential flow

In the full compressible inviscid equations of motion (Euler) a flow around a sharp corner or an edge with a small radius of curvature will always cause expansion to supersonic flow. Compression to the point where the flow is leaving the surface in Fig. 5 now can only happen through a shock which will cause total pressure loss and a rise in entropy.

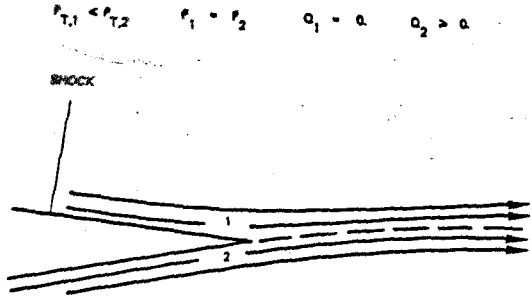

Fig. 6: Trailing edge flow in compressible Euler flow

This will require a point on the surface with different total pressure which implies different velocities for the same static pressure, i.e. a contact discontinuity or wake. However, this solution is not stable since there exists in subsonic flow a solution without any total pressure loss, namely the one with the flow leaving the trailing edge and thus not having the large expansion and the shock. In transonic lifting cases with shocks, the total pressure loss on one side is larger than on the other which will only allow the flow to stagnate at the trailing edge upper surface while the velocity at the training edge lower surface is finite, thus leaving the lower surface smoothly as shown in Fig. 6. The wake contact discontinuity in velocity and total pressure is captured in the fully conservative finite volume scheme. Therefore the wake shape is not fixed due to the mesh but will be a result independent of the mesh chosen.

Different two-dimensional numerical experiments on airfoils with subcritical flow proved that this phenomenon does not depend on the initial solution. Even with a fully converged potential flow solution forced to have $C_L = 0$ as starting solution the Euler time stepping method on the same mesh gave the $C_L \neq 0$ converged solution identical to the one starting from undisturbed flow. The same experiments showed no basic influence of the dissipative terms added. O or C meshes do not change the results. Flow leaving the trailing edge smoothly seems to be the only stable Euler solution without having something different enforced.

The same mechanisms applies to sharp leading or side edges or when the radius of curvature is small combined with locally supersonic flow.

4. CONVERGENCE ACCELERATION

Different devices can be used to accelerate the convergence of the solution to a steady state.

The techniques presented here have the advantage that they allow a high degree of vectorization on present day vector computers.

In order to modify the speed of wave propagation in explicit schemes without altering the steady state one can multiply the terms containing the space derivatives by a matrix M to produce the equation

$$\frac{\partial U}{\partial t} + M\left\{ \frac{\partial F_1}{\partial x} + \frac{\partial F_2}{\partial y} + \frac{\partial F_3}{\partial z} \right\} = 0 \qquad (50)$$

If we restrict M to be of the form λI, where λ is a scalar multiplier, then one can choose λ so that the equations are advanced at the maximum Courant number permitted by the difference scheme at every point in the domain. This is equivalent to using different time steps at different points. Since the present time stepping schemes are so constructed that the steady state is independent of the time step, consequently the time step can be altered from one point to the next without altering the steady state. This simple technique gives at least an order of magnitude convergence acceleration, in general, compared with the classical time accurate minimum time stepping. This technique is standard in all our codes unless time accuracy is required.

The solutions of the Euler equations have constant enthalpy in the steady state. If our interest is only in the steady state we could assert that H will always be H_∞ even in the transient phase and then solve the non-physical system of equation by $H = H_\infty$. Physically this would correspond to a flow with local energy supply to freeze H. This approach has been used, e.g. in Ref. [25]. Its main advantage is the reduction in storage requirement and computational work. An alternative which we followed extensively is to use the difference in total enthalpy in the transient state as a driving mechanism to accelerate convergence. Details can be found in Ref. [30]. This damping technique is very similar to the turning of the unsteady potential equation into a kind of telegraph equation which has damped waves as its fundamental solutions. Fig. 7b portrays the convergence history for the NACA 0012 with enthalpy damping and local time stepping. Direct comparison of Fig. 7a with Fig. 7b gives an impression of the convergence acceleration.

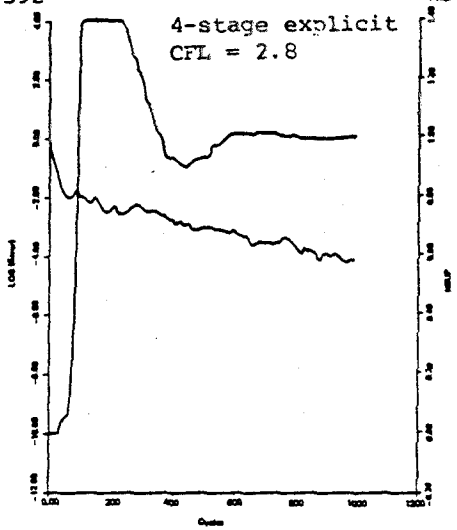

Fig. 7a: Convergence history without enthalpy damping

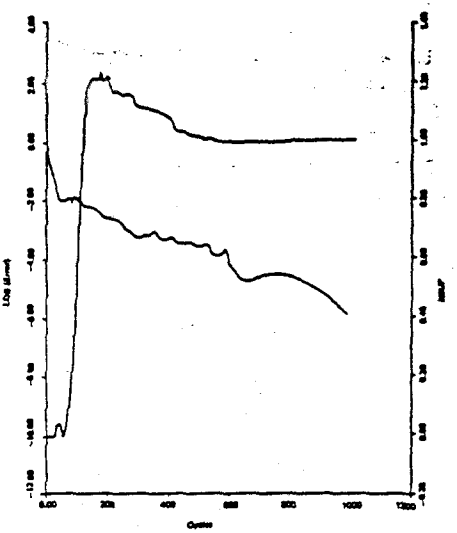

Fig. 7b: Convergence history with enthalpy damping

Another approach is to increase the permissible time step by using an implicit scheme. Implicit approximate factorization methods have been widely used. These are described in detail by R.M.Beam [27]. MacCormack has also developed a new implicit scheme by adding implicit stages to his earlier explicit scheme [28]. This allows the use of very longer time steps, and has proved quite effective for Navier Stokes calculations.

An attractive alternative approach is to drive an explicit scheme by averaged residuals. Consider the model problem

$$U_t + aU_x + V \cdot a \cdot \Delta x^3 \, U_{xxxx} = 0 \qquad (51)$$

With $\lambda = a\Delta t/\Delta x$ the residual is

$$R_i = \lambda \{ (U_{i+1} - U_{i-1}) - V(U_{i+1} - 4U_{i+1} + 6U_i - 4U_{i-1} + U_{i-2}) \} \qquad (52)$$

Now replace R_i by the averaged residual

$$\bar{R}_i = \varepsilon R_{i-1} + (1-2\varepsilon) R_i + \varepsilon R_{i+1}$$

$$= (1+\varepsilon\delta_x^2) R_i \qquad (53)$$

in the time stepping scheme. A four stage scheme with averaging is as follows marching from time level n to n+1

$$
\begin{aligned}
U^{(0)} &= U^n \\
U^{(1)} &= U^{(0)} - (\Delta t/4)\bar{R}^{(0)} \\
U^{(2)} &= U^{(0)} - (\Delta t/3)\bar{R}^{(1)} \\
U^{(3)} &= U^{(0)} - (\Delta t/2)\bar{R}^{(2)} \\
U^{(4)} &= U^{(0)} - \Delta t\, \bar{R}^{(3)} \\
U^{n+1} &= U^{(4)}
\end{aligned}
\tag{54}
$$

Assuming an infinite interval and taking the Fourier transform this scheme has the amplification factor

$$g = 1 - \zeta + \zeta^2/2 - \zeta^3/6 + \zeta^4/24 \tag{55}$$

with the Fourier symbol

$$\zeta = \lambda \{i \sin\xi + 4V(1-\cos\xi)^2\} \{1-2\varepsilon(1-\cos\xi)\} \tag{56}$$

The second factor represents the smoothing due to the averaging, and allows λ to be increased.

To remove the restriction on the smoothing constant one can perform residual averaging implicitly

$$(1-\varepsilon\delta_x^2)\, \bar{R}_i = R_i$$

or

$$-\varepsilon\bar{R}_{i-1} + (1-2\varepsilon)\, \bar{R}_i - \varepsilon\bar{R}_{i+1} = R_i$$

On an infinite interval this has the solution

$$\bar{R}_i = (1-r)/(1+r) \{R_i + r(R_{i-1}+R_{i+1}) + r^2(R_{i-1}+R_{i+2}) + \dots\} \tag{58}$$

where $\varepsilon = r/(1-r)^2 \quad , r < 1$ (59)

Now one finds it sufficient for stability that

$$\varepsilon \geq 1/4 \{(\lambda/\lambda^*)^2 - 1\} \tag{60}$$

where λ^* is the Courant number limit for the unsmoothed scheme. In terms of the decay parameter r the stability condition is

$$(1+r)/(1-r) \geq \lambda/\lambda^* \tag{61}$$

On the stability limit this is equivalent to summing the residuals along a line with the original time step

$$\bar{R}_i = R_i + r(R_{i-1}+R_{i+1}) + r^2(R_{i-2}+R_{i+2}) + \ldots \tag{62}$$

Since

$$1 + r\cos\xi + r^2\cos 2\xi + \ldots = (1-r\cos\xi)/(1-2r\cos\xi+r^2) \tag{63}$$

the Fourier transform in the absence of dissipation is

$$g = 1 - \zeta + \zeta^2/2 - \zeta^3/6 + \zeta^4/24 \tag{64}$$

where

$$\zeta = \lambda \frac{(1-r^2)\sin\xi}{1-2r\cos\xi+r^2}, \qquad |\zeta| \leq \lambda \tag{65}$$

Fig. 8 shows results for the NACA 0012 section at M = 0.80, $\alpha = 0^\circ$ for a 128x32 O-mesh with implicit residual averaging at CFL = 8.0.

The comparison with Fig. 7 clearly shows the improvements in convergence speed. Both flow field resutls are identical:

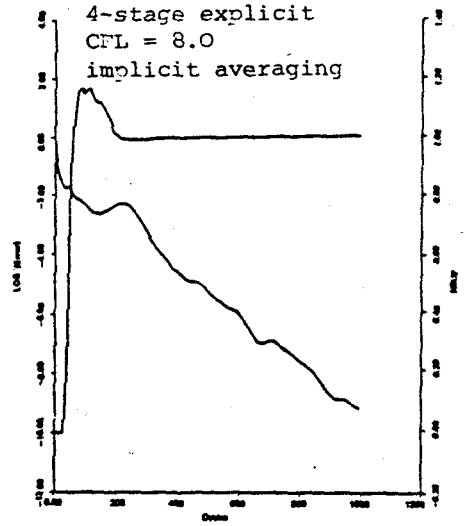

Fig. 8: Convergence histories with implicit residual averaging

The final acceleration technique is the multiple grid technique which has been demonstrated already in a previous chapter to be a very powerful tool for quasi-linear second order differential equations. Brandt [31] proposed a multi-grid solver for the steady Euler and Navier-Stokes equations, while Ni [32] presented a multiple grid technique based on a one step distribution formula scheme for the Euler equations. We have tried several multigrid techniques since late 1980 in combination with a cell-center as well as nodal point time stepping scheme and with a Ni-type one step scheme [33]. First results on the multistage time stepping scheme with multigrid acceleration have been presented in Ref. [34]. This procedure can be described as follows:

The basic idea is to use the coarser grids to propagate the fine grid corrections properly and rapidly through out the field, thus improving convergence rate to steady state while maintaining low truncation errors by using the fine grid discretisation.

The changes ΔU_{2h} in the coarse grid, obtained by removing every other line from the fine grid, are determined by

$$\Delta U_{2h} = I_{2h}^{h} \, \delta U_{h} \tag{66}$$

Where I_{2h}^{h} is an operator which transfers to each control volume of the coarse grid the correction δU_{H} of the fine grid using a distribution formula.

After computing the corrections δH_{2h} on all coarse grid points the flow properties at the finest grid are updated by

$$U^{h} = U + I_{h}^{2h} \, \delta U_{2h}$$

where I_{h}^{2h} is a linear interpolation operator which interpolates the coarse grid corrections to give the corrections at each fine grid point of the finest mesh.

Let P be the space difference operator. The subscripts h, 2h denote fine and coarse meshes. The initial value and the forcing term for the coarse mesh are defined by

$$U_{2h}^{(0)} = Q_{2h}^{h} \, U_{h}^{n} \quad , \quad F_{2n} = \bar{Q}_{2h}^{h} \, P_{h} \, U_{h}^{n} - P_{2h} \, U_{2h}^{(0)} \tag{68}$$

where Q_{2h}^{h} and $\bar{Q}_{2h}^{h}$ are collection operators. During the time stepping process we advance on the coarse mesh by

$$
\begin{aligned}
U_{2h}^{(1)} &= U_{2h}^{(0)} - \alpha_1 \Delta t_{2h} \left(P_{2h} U_{2h}^{(0)} + F_{2h}\right) \\
U_{2h}^{(2)} &= U_{2h}^{(0)} - \alpha_2 \Delta t_{2h} \left(P_{2h} U_{2h}^{(1)} + F_{2h}\right) \\
U_{2h}^{(3)} &= U_{2h}^{(0)} - \alpha_3 \Delta t_{2h} \left(P_{2h} U_{2h}^{(2)} + F_{2h}\right) \\
U_{2h}^{(4)} &= U_{2h}^{(0)} - \Delta t_{2h} \left(P_{2h} U_{2h}^{(3)} + F_{2h}\right)
\end{aligned}
\tag{69}
$$

Then U_h on the fine mesh is updated by

$$
U_h^{n+1} = U_h + R_h^{2h} \{U_{2h}^{(4)} - U_{2h}^{(0)}\} \tag{70}
$$

where R_h^{2h} is an interpolation operator.

The corresponding multi-grid sequence is shown in Fig. 9.

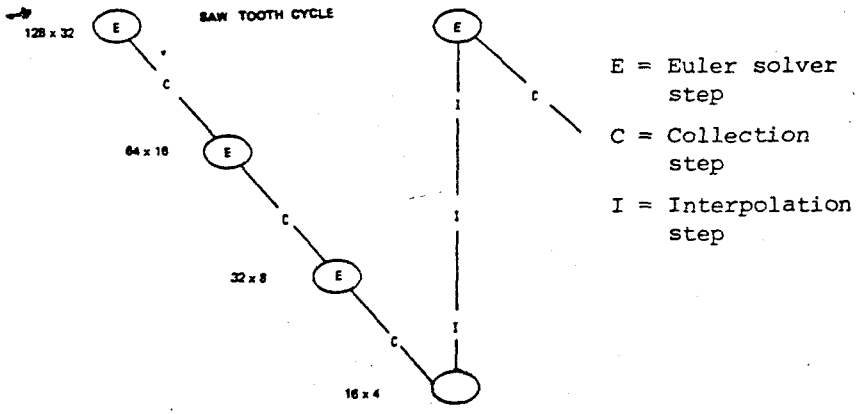

Fig. 9: Multi-grid cycle for multigrid Euler time stepping (METS) scheme

On Fig. 10 the convergence history is depicted for the NACA 0012 test case as before.

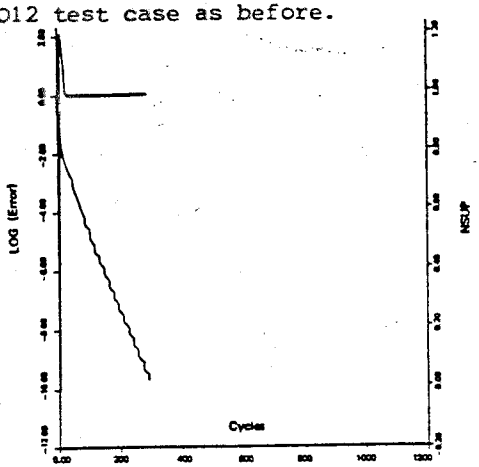

10: Convergence history for METS-scheme CFL = 2.2

The improvement in convergence speed is quite impressive ared with the results shown in Fig. 7 and Fig. 8. Further oles and pressure distributions are shown in section 6.

MESH GENERATION

The numerical schemes presented in this chapter can be for the computation of complete three-dimensional aircraft fields. However, the problems of geometry discretiation iesh generation presently limit the complexity of the con- :ations which can be treated. Mesh generation is a diffi- and rather lenghty problem, and will not be discussed in detail. Ref. 35-39 give an overview over the present e of the art.

The accuracy and physical relevance of a numerical solu- depends on the capability of the mesh to resolve both, geometry and the details of the flow. Large surface cur- :e and rapid variations of the flow variables require meshes. Rather than using very fine meshes everywhere, :ive grids and interactive mesh generation under visual :ol have to be developed.

RESULTS

Large number of two- and three-dimensional computations been performed, e.g. see Ref. [1], [25], [26], [40] - Some typical results are shown to demonstrate the ac- :y and convergence of the basic numerical algorithm as as results to show the wide range of possible .cations.

6.1 Two-Dimensional Flows

Two typical results are presented for the NACA 0012 airfoil section. Both have been obtained on a 320x64 O-mesh. Fig. 11 shows the static pressure distribution and the iso-Mach lines for $M = 0,8^{\circ}$, $\alpha = 1.25^{\circ}$.

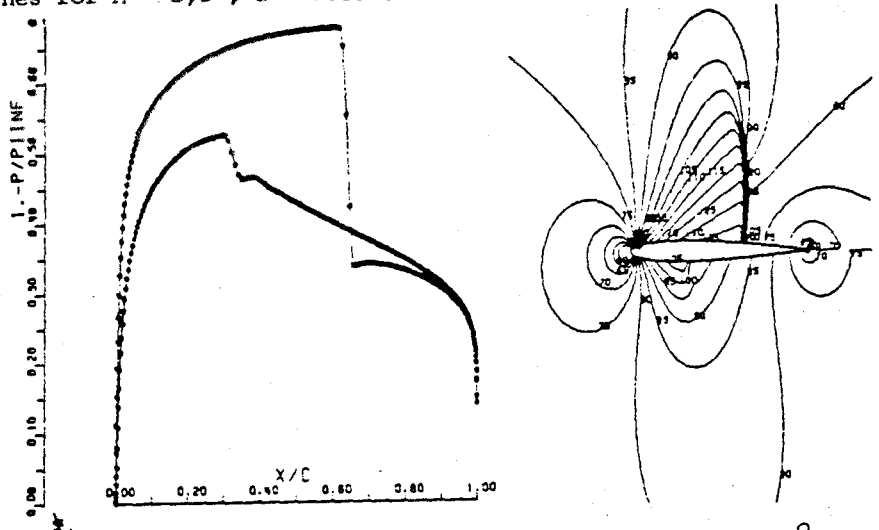

Fig. 11: Results for the NACA 0012, $M = 0,80$, $\alpha = 1.25^{\circ}$

To prove the accuracy of the present solution, the total pressure losses in the airfoil nose region are plotted on Fig. 12. These spurious losses based on the numerical scheme and the boundary conditions are less than a tenth of a percent.

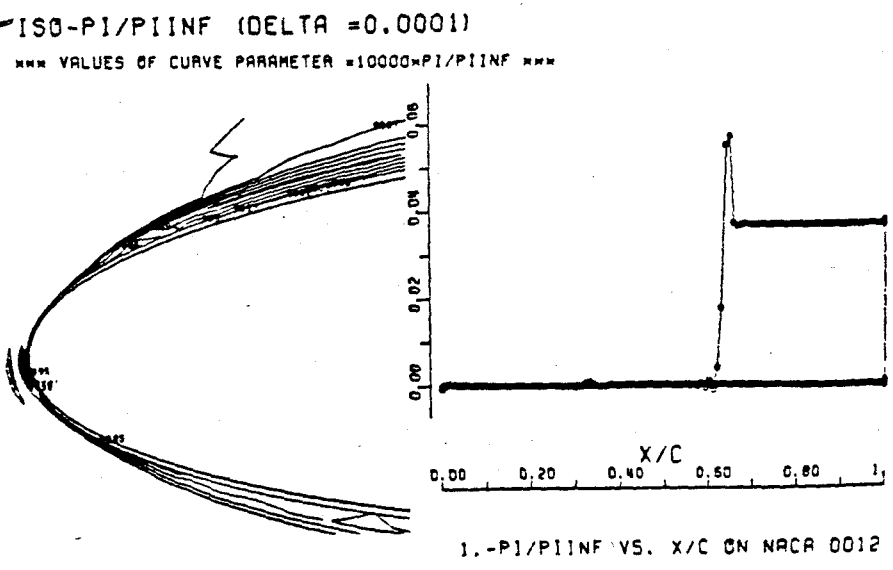

Fig. 12: Total pressure losses in the nose region NACA 0012, $M = 0.80$, $\alpha = 1.25^{\circ}$

To demonstrate the subsonic as well as supersonic capabilities of the present approach, on Fig. 13 corresponding results are presented for the NACA 0012 at M = 1.2, $\alpha = 7^{\circ}$.

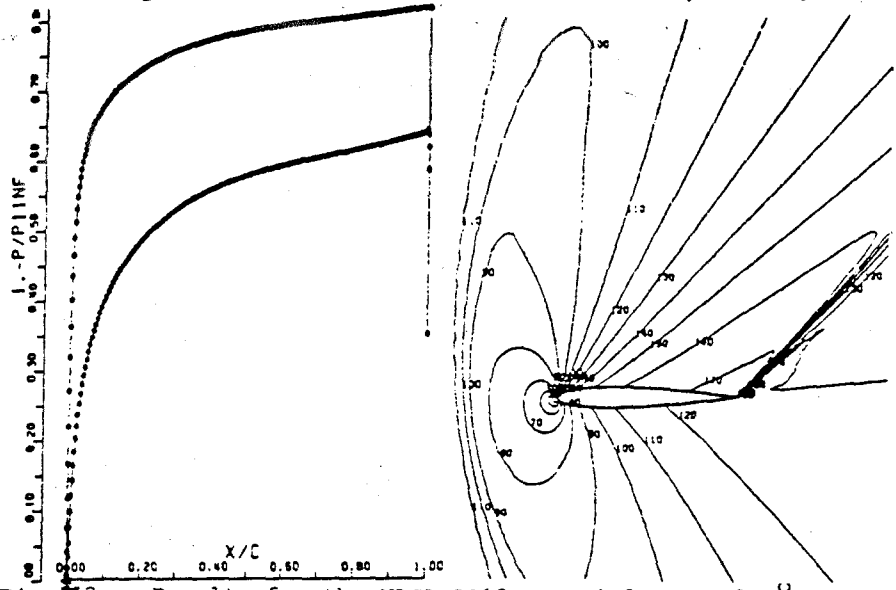

Fig. 13: Results for the NACA 0012, M = 1.20, $\alpha = 7.0^{\circ}$

The detached bow shock as well as the oblique shock at the upper surface trailing edge are nicely resolved.

6.2 Three-Dimensional Flow

The variety of configurations analysed so far ranges from cars to transport and fighter wing-body combinations, from transport aircraft nacelles or complete turbo-propulsion-simulators to fighter air intakes and from propeller thrust and swirl simulations to rocket plume distortions from fired missiles on air intakes. We limit ourselves here to two rather attractive applications, namely leading edge vortex flows and air intake flow.

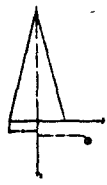

HUMMEL-EXPERIMENT

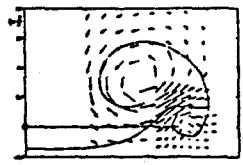

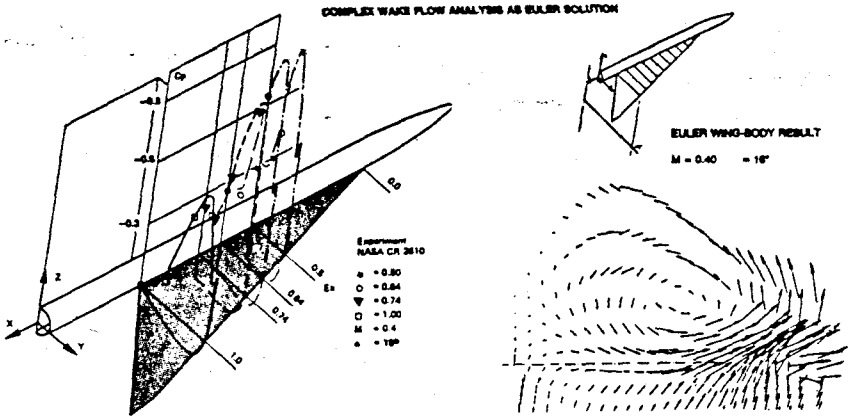

Fig. 14: Leading edge vortex flow analysis, Ref. [42]

New generations of fighter aircraft should have excellent transonic manoeuver capabilities and also be capable of sustained supersonic cruise and manoeuver. This requires excellent tools for wing leading and trailing edge design including flaps to control vortex flow and vortex burst. Fig. 14 shows some results which demonstrate the capabilities of Euler solutions.

Another interesting task is the analysis of missile plume effects during missile launch on the air intake of the carrier plane. This is necessary to predict possible flow distortion in the intake duct, and especially at the compressor entrance.

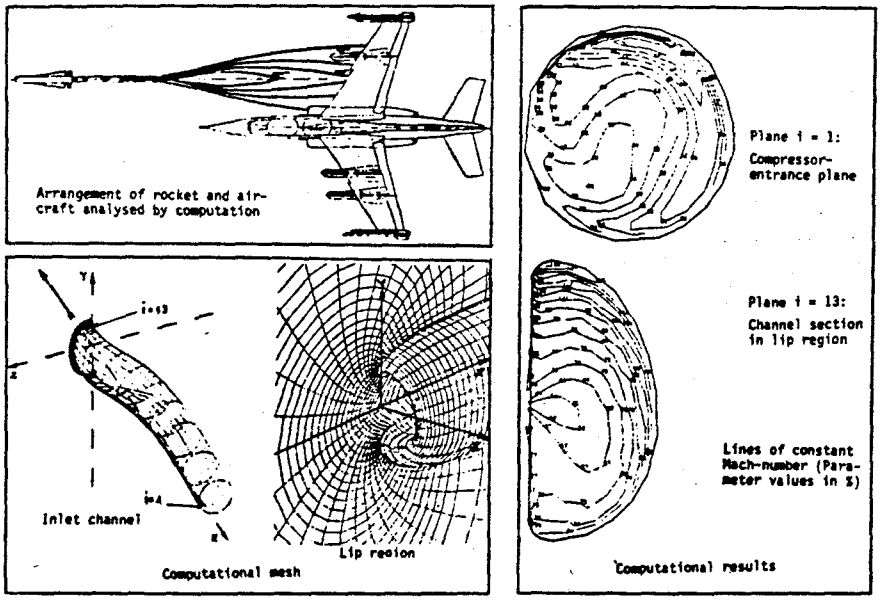

Fig. 15: Intake distortion due to missile launch, Ref. [44]

Fig. 15 portrayes some results of the Euler-analysis of this very complex problem. The three-dimensional side-mounted air-intake at the fuselage has been discretized together with the complete curved duct. Such numerical simulations are very helpful in preparing expensive and risky flight tests. Computer time for such a case is less than 10 min CPU on a CRAY 1 vector computer.

7. CONCLUSIONS

Advances in solution algorithms and complex mesh generation strategies have led to effective Euler methods. These provide a very attractive and important tool in aircraft analysis and design. The approach presented in this chapter combines high accuracy and fast convergence. It can also be readily extended to the Navier Stokes equations. The high degree of vectorization is well suited for vector computers like CRAY.

8. REFERENCES

[1] HAASE, W., WAGNER, B., JAMESON, A., and SCHMIDT, W. - Development of a Navier-Stokes Method Based on Finite Volume Techniques for Solving the Time-Dependent Euler Equations. 5th GAMM-Conference on Numerical Methods in Fluid Mechanics, Roma, Italy, Oct. 1983.

[2] WAGNER, B., and SCHMIDT, W. - Theoretical Investigations of Real Gas Effects in Cryogenic Wind Tunnels. AIAA Journal, Vol. 16, pp. 584-586, 1978.

[3] KUTLER, P., RAINHARDT, W.A., and WORMING, R.F. - Numerical Computation of Multishocked, Three-Dimensional Supersonic Flow Fields with Real Gas Effects. AIAA Paper 72-702, 1972.

[4] VIVIAND, H. - Formes Conservatives des equations de la dynamique des gaz. La Rech. Aerosp. No. 1971-1, 1974, pp 65-66.

[5] LAX, P.D. - Weak Solutions of Nonlinear Hyperbolic Equations and Their Numerical Computation. Comm. Pure and Appl. Math., Vol. 7. 1954.

[6] MacCORMACK, R.W. - The Effect of Viscosity in Hypervelocity Impact Cratering. AIAA Paper 69-354, 1969

[7] LAX, P.D., and WENDROFF, B. - Difference Schemes for Hyperbolic Equations with High Order of Accuracy. Comm. Pure and Appl. Math., Vol. 17, 1964.

[8] GARY, J. - On Certain Finite Difference Schemes for Hyperbolic Systems. Math. Comp., Vol. 18, pp. 1-18, 1964.

[9] STETTER, H.J. - Improved Absolute Stability of Predictor-Corrector Schemes, Computing, Vol. 3, pp. 286-296, 1986.

[10] GRAVES, R. and JOHNSON, N. - Navier Stokes Solutions Using Stetter's Method. AIAA Journal, Vol. 16, pp. 1013-1015, 1978.

[11] KREISS, H.O. - Initial Boundary Value Problems for Hyperbolic Systems. Comm. Pure Appl. Math., Vol. 23, pp. 277-298, 1970.

[12] GOTTLIEB, D. and TURKEL, E. - Boundary Conditions for Multistep Finite Difference Methods for Time Dependent Equations. J. Computational Physics, Vol. 26, pp. 181-196, 1978

[13] GUSTAFSSON, B. and OLIGER, J. - Stable Boundary Approximations for a Class of Time Discretizations of $u_t = AD\,u$. Upsala University, Dept. of Computer Sciences, Report 87, 1980.

[14] RUDY, D. and STRIKWERDA, J. - A Non-reflecting Outflow Boundary Condition for Subsonic Navier Stokes Calculations. J. Computational Physics, Vol. 36, pp. 55-70, 1980.

[15] PORTER, R.W. and COAKLEY, J.F. - Use of Characteristics for Boundaries in Time Dependent Finite Difference Analysis of Multidimensional Gas Dynamics. Int. J. Num. Meth. in Engineering, Vol. 5, 1972, pp. 91-101.

[16] RIZZI, A.W. - Charakteristische Gleichungen für quasizeitabhängige Euler Verfahren. Dornier Note BF 30-1496/79, 1979.

[17] GRASHOF, J. - Charakteristikenbezeichnungen für die dreidimensionalen zeitabhängigen Euler-Gleichungen bei konstanter Gesamtenthalpie. Dornier Note BF 30-1512/79, 1979.

[18] GRASHOF, J., SCHMIDT, W. and RIZZI, A.W. - Verfahren zur Berechnung der reibungsfreien Strömung an Überschalleinläufen. DORNIER FB 80/44B, 1980.

[19] ENGQUIST, B. and MAJDA, A. - Absorbing Boundary Conditions for the Numerical Simulation of Waves, Math. Comp. Vol. 31, pp. 629-651, 1977.

[20] BAYLISS, A. and TURKEL, E. - Outflow Boundary Conditions for Fluid Dynamics. ICASE Report 80-21, 1980.

[21] RIZZI, A. - Numerical Implementation of Solid Body Boundary Conditions for the Euler Equations. ZAMM Vol. 58, pp. 301-304, 1978.

[22] MacCORMACK, R.W. and WARMING, R.F. - Survey of Computational Methods for Three-Dimensional Supersonic Inviscid Flows with Shocks. AGARD-LS-64, Paper 5, 19, 1973.

[23] SCHMIDT, W. - Wall Boundary Conditions for Cell Centered Finite Volume Schemes. Dornier Note BF-2445/83, 1983.

[24] MANGLER, K.W. and SMITH, J.H.B. - Behaviour of the Vortex Sheet at the Trailing Edge of a Lifting Wing. RAE TR 69049, 1969.

[25] SCHMIDT, W., JAMESON, A. and WHITFIELD, D. - Finite Volume Solutions to the Euler Equations in Transonic Flow. Journal of Aircraft, Vol. 20, No. 2, pp. 127-133, 1983.

[26] SCHMIDT, W., JAMESON, A. - Euler Solutions as Limit of Infinite Reynolds Number for Separated Flows and Flows with Vortices. In: Lecture Notes in Physics Vol. 170, Ed. E. Krause, pp. 468-473, Springer Verlag, 1982.

[27] BEAM, R.M. - Implicit Numerical Methods for the Compressible Navier Stokes and Euler Equations. VKI-Lecture Series 1982, March 29-April 2, 1982.

[28] MacCORMACK, R.W. - A Numerical Method for Solving the Equations of Compressible Viscous Flow. AIAA-Paper 81-0110, 1981.

[29] VIVIAND, H. and VEUILLOT, J.P. - Méthodes Pseudo-Instationnaires Pour le Calcul D'Ecoulements Transsoniques. ONERA Publication No. 1978-4, 1978.

[30] JAMESON, A., SCHMIDT, W., TURKEL, E. - Numerical Solutions for the Euler Equations by Finite Volume Methods Using Runge Kutta Time Stepping Schemes. AIAA-Paper 1259, June 1981.

[31] BRANDT, A. - Multigrid Solutions to Steady-State Compressible Navier-Stokes Equations I. Proc. 5th Int. Comp. Meth. in Appl. Science and Engin., Dec. 1981.

[32] NI, Ron-Ho. - A Multiple Grid Scheme for Solving the Euler Equations. AIAA-Paper 81-1025, 1981.

[33] SCHMIDT, W. and JAMESON, A. - Application of Multi-Grid Methods for Transonic Flow Calculations. In: Lecture Notes in Mathematics Vol. 960, Ed. W. Hackbusch and U. Trottenberg, pp. 599-613, Springer Verlag, 1982.

[34] JAMESON, A. - A Multi-Grid Solution Method for the Euler Equations. Int. Multigrid Conference, Copper Mountain, Colorado, April 1983.

[35] NASA, Ed. - Numerical Grid Generation Techniques. NASA-CP 2166, 1980.

[36] RIZZI, A.W. and ERIKSSON, L.E. - Transfinite Mesh Generation and Damped Euler Equation Algorithm for Transonic Flow Around Wing-Body Configurations. AIAA Paper 81-0999, 1981.

[37] WARSI, Z. - Tensor and Differential Geometry Applied to Analytic and Numerical Coordinate Generation. MSSU-EIRS-81-1, 1981 Mississippi State University

[38] LEE, K.D. - 3-D Transonic Flow Computations Using Grid Systems with Block Structure. AIAA Paper 81-0998, 1981.

[39] LEICHER, S., FRITZ, W., GRASHOF, J. and LONGO, J. - Mesh Generation Strategies for CFD on Complex Configurations. In: Lecture Notes in Physics Vol. 170, Ed. E. Krause, pp. 329-334, Springer Verlag, 1982.

[40] SCHMIDT, W. and JAMESON, A. - Recent Developments in Finite Volume Time-Dependent Techniques for Two- and Three-Dimensional Transonic Flows. In: Von Karman Institute Lecture Series 1982-04, Computational Fluid Dynamics, March 1982, Brussels.

[41] GRASHOF, J. and SCHMIDT, W. - Computational Methods for Two- and Three-Dimensional Inlets in Subsonic and Supersonic Flows. In: 13th ICAS Congress, Seattle, Aug. 1982.

[42] HITZEL, S. and SCHMIDT, W. - Slender Wings with Leading Edge Vortex Separation - A Challenge for Panel-Methods and Euler-Codes. AIAA-Paper 83-0562, AIAA 21st Aerospace Sciences Meeting, Jan. 1983.

[43] SCHMIDT, W. - Advanced Numerical Methods for Analysis and Design in Aircraft Aerodynamics. Int. J. of Vehicle Design, Technological Advances in Vehicle Design Series, SP6, Application of New Techniques for Analysis and Design of Aircraft Structures, 1983.

[44] GRASHOF, J. - Numerical Investigation of Three-Dimensional Transonic Flow Through Air Intakes Disturbed by a Missile Plume. AIAA-Paper 83-1854, July 1983.

[45] CHAN, H.C., RUBBERT, P.E., YU, N.J. and JAMESON, A. - Flow Simulation for General Nacelle Configurations Using Euler Equations. AIAA-Paper 83-0539, Jan. 1983.

[46] WHITFIELD, D. and JAMESON, A. - Three-Dimensional Euler Equation Simulation of Propeller Wing Interaction in Transonic Flow. AIAA-Paper 83-0236, Jan. 1983.